

Upper critical fields in liquid-quenched metastable superconductors

K. M. Wong,* E. J. Cotts,[†] and S. J. Poon**Department of Physics, University of Virginia, Charlottesville, Virginia 22901*

(Received 4 April 1984)

A systematic and quantitative study of upper critical fields in alloys with increasing atomic number is carried out. The alloys are prepared by the technique of liquid (splat) quenching. They include the metastable body-centered-cubic (β) phase of Ti-Pd, Zr-Mo, Zr-Pd, and Hf-Mo, amorphous phase of Zr-Rh, and the stable β phase of Ti-Mo and Ta-Hf. Measurements are made in magnetic fields up to 90 kG and in temperatures down to 0.5 K. The results are analyzed within the framework of the dirty-limit theory of Werthamer, Helfand, Hohenberg, and Maki (WHHM). A least-squares fitting routine is performed using *all the data* (weighted equally) for a given sample. It is emphasized that the visual critical-field gradient near the transition temperature cannot be taken as the actual gradient in the presence of Pauli paramagnetic limitation. The main findings are the following: (i) Even without including renormalization corrections due to electron-phonon and electron-electron interactions, very good fits to the WHHM theory are obtained; (ii) critical-field data for all our samples (with minor exceptions in Hf-Mo) are found to fall below or on the Maki curve (i.e., when the spin-orbit scattering parameter $\lambda_{s.o.}$ goes to infinity); (iii) values of $\lambda_{s.o.}$ are observed to range from 0.28 to 2.51 for the 3d and 4d alloys; (iv) the spin-orbit scattering rates $1/\tau_{s.o.}$ are found to compare well with theoretical estimation using results from band-structure calculation. The effect of sample inhomogeneity on the value of $\lambda_{s.o.}$ in Zr-Mo alloys is also illustrated. Inclusion of renormalization effects in several alloys yields somewhat reduced (at most by a factor of ~ 2 in Ti-V) values of $\lambda_{s.o.}$. Incorporating the strong-coupling correction intuitively into the theory does not seem to have an overall effect on the values of $\lambda_{s.o.}$.

I. INTRODUCTION

Experimental study of superconductors in high magnetic fields during the last two decades has been closely coupled with the development of detailed theory. The interactions of magnetic field with the motion and spin of the electrons of the Cooper pairs in superconductors, and the spin-orbit interaction, have been revealed to be significant in determining critical-field behavior. The theoretical development of Maki¹ predicted an upper bound (the Maki curve) on critical fields $H_{c2}(T)$ as a result of orbital pair breaking. The further limitations of $H_{c2}(T)$ by Pauli paramagnetism were subsequently quantified by Werthamer, Helfand, and Hohenberg² along with the restorative effects on $H_{c2}(T)$ of the spin-orbit interaction. The Werthamer, Helfand, Hohenberg, and Maki (WHHM) theory was developed for weak-coupled, homogeneous, dirty superconductors. Comparison of theory with critical-field data was based on a two-parameter (α and $\lambda_{s.o.}$ representing Pauli paramagnetic limitation and spin-orbit scattering, respectively) curve-fitting procedure. As interest in critical fields has increased and data for a greater variety of superconductors have been achieved, refinement of theory has followed. Extension of the theory to include strong coupling has been attempted by Rainer and Bergmann.³ Further refinement of the theory has included the effects of the electron-phonon interaction and electron-spin fluctuations, via a renormalization procedure as suggested by Orlando *et al.*⁴ The WHHM theory and developments can be found in several publications.^{5,6}

In this paper we report results obtained from a sys-

tematic and quantitative study of upper critical fields in metastable transition-metal-alloy superconductors. The latter class of materials offers an excellent opportunity for the extensive study of upper critical-field behavior $H_{c2}(T)$ and to test the predictions of the WHHM theory. Generally these samples satisfy the "dirty limit." Employing the technique of liquid quenching, a large variety in the selection of the sample constituents which form a "single phase" can be attained, easily including transition metals from the fourth, fifth, and sixth rows of the Periodic Table (3d, 4d, and 5d series). Thus the spin-orbit scattering rate, a determining factor in the WHHM theory, can be varied. Samples of good homogeneity can be produced or the degree of homogeneity can be varied [so as to study the effect of inhomogeneity upon $H_{c2}(T)$]. Samples of varying superconducting transition temperature are attained (2.7 to 6.6 K). As a result, we are able to test the applicability of the WHHM theory in a variety of suitable samples, varying the parameters relevant to the WHHM theory over a wide range. We find that the WHHM theory provides good fits to the data for all samples, i.e., all our $H_{c2}(T)$ data fall on or below the theoretical Maki curve. The renormalization procedure suggested by Orlando *et al.*^{4,6} can also be applied and similarly good fits to the data are produced. The parameter estimates provided by the data analysis are in good agreement with theoretical estimates. The format of this paper is as follows. In Sec. II experimental procedures are given. Section III presents experimental results, analysis, and discussion. Section IV is the summary and conclusion.

TABLE I. Superconducting and normal-state parameters for all the alloys discussed in the text. No renormalization correction is taken into account. ΔT_c denotes transition width defined by the 0% and 90% points on the resistivity curve. The spin-orbit coupling matrix elements squared ξ_d^2 for the d band are taken from Ref. 13. The $Zr_{96}Mo_4$ sample contains traces of α and ω phases.

Alloys	ρ_n ($\mu\Omega$ cm)	T_c (K)	ΔT_c (mK)	α_{visual}	α	$\lambda_{\text{s.o.}}$	$\lambda_{\text{s.o.}} T_c$ (K)	ξ_d^2 (element) (meV) ²
Ti ₄₂ V ₅₈ ^a	59	7.52		1.58	1.84	0.28	2.11	~420 (Ti,V)
Ti ₈₅ Mo ₁₅	115	4.08	60	1.64	1.86	0.64	2.61	
Ti ₈₅ Pd ₁₅	210	3.82	60	1.99	2.20	0.65	2.48	
Ti ₅₆ Nb ₄₄ ^a	53	8.99		1.35	1.51	1.33	11.5	
Zr ₇₅ Rh ₂₅ (as-quenched)	160	4.30	5	1.50	1.79	1.84	7.91	~3600 (Zr)
Zr ₇₅ Rh ₂₅ (annealed)	155	3.97	5	1.58	1.76	1.69	6.71	
Zr ₈₅ Pd ₁₅	130	4.80	20	1.25	1.40	2.51	12.0	
Zr ₉₃ Mo ₇	130	4.91	550	1.06	1.20	2.00	9.82	
Zr ₉₆ Mo ₄	119	4.47	540	0.89	0.98	∞	∞	
Hf _{90.6} Mo _{9.4}	165	2.71	230	1.19	1.30	∞	∞	~36 000 (Hf)
Ta ₇₅ Hf ₂₅	60	6.62	100	0.64	0.68	∞	∞	~60 000 (Ta)

^aData taken from Ref. 11; see text for analysis of data.

II. EXPERIMENTAL

The samples examined in this study are all transition-metal binary alloys (see Table I). Alloy constituents were selected from the $3d$, $4d$, and $5d$ transition metals, with superconducting transition temperatures of the alloys ranging from 2.7 to 6.6 K. The majority of the samples were produced by quenching onto a copper plate at a glancing angle. The copper plate was heated to 180°C in an argon atmosphere. Foils 40 to 100 μm thick were produced. Alloys of Zr-Pd, Zr-Mo, and Hf-Mo were liquid-quenched in this manner, while Ti-Mo and Ta-Hf did not require as high a cooling rate. The Ti-Pd samples were produced by a modified piston-anvil technique. All the above-mentioned alloys were produced in metastable, body-centered-cubic (β -phase) crystal structures. Details of sample preparation (and alloy structures) have been provided previously.⁷ The $Zr_{75}Rh_{25}$ samples were amorphous, produced by melt spinning in vacuum.

X-ray (Ni-filtered Cu $K\alpha$ radiation) analysis indicated that the samples were single phase, except for $Zr_{96}Mo_4$ which contained traces of α and ω phases. The latter was intentionally selected so as to study the effects of inhomogeneity upon H_{c2} . Four terminal measurements of the zero-field superconducting transition of samples revealed transition widths (defined by the 0% and 90% points on the resistivity curve) of 5 to 500 mK (see Table I). The samples were in the form of long, thin strips generally of thickness ~ 40 μm , width ~ 0.1 cm, and length ~ 1 cm. Thin (0.01 cm diameter) copper leads were welded to the samples to facilitate four terminal resistivity measurements.

Measurements of critical fields $H_{c2}(T)$ were undertaken at fields up to 90 kG and temperatures down to 0.5 K. A superconducting magnet with a 3-cm-diam, 3-cm-long homogeneous (0.2%) space was utilized. Three different refrigeration techniques were employed. Primary thermometry in all cases was provided by a calibrated Ge ther-

mometer.⁸ At temperatures above 4.2 K the sample and sample holder were enclosed in (and thermally grounded to) a copper can, with a copper extension in contact with a ⁴He bath.⁹ Secondary thermometry, in magnetic fields, was provided by a capacitive thermometer, which also was used (with a properly positioned heater)⁹ for temperature regulation. Between 1.5 and 4.3 K the samples and sample holder were immersed in a pumped liquid ⁴He bath. Secondary thermometry was provided by measurement of the vapor pressure. Between 0.5 and 1.6 K samples and sample holder were immersed in a pumped ³He bath. Secondary thermometry was provided by measurement of vapor pressure. Good agreement [smooth-fitting $H_{c2}(T)$ curves and agreement (1%) of overlapping data points] was observed between different temperature regimes.

All measurements were taken with the samples, and thus current density J , parallel to the field ($J||B$). Current densities were at all times less than 1 A/cm². The magnetic field was swept at a constant positive rate of 6 kG/sec. For a given sweep, the 50% point (midpoint) and the extrapolated 0% point (end point) of the resistive transition upon increasing fields were recorded (see Fig. 1).

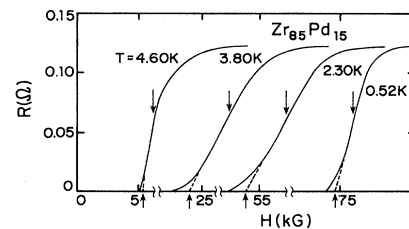


FIG. 1. Resistance as a function of magnetic field for a $Zr_{85}Pd_{15}$ sample at four temperatures. Dashed lines extrapolate to zero resistance. Up- and down-pointing arrows indicate 0% and 50% points on the transition curves, respectively.

III. RESULTS, ANALYSIS, AND DISCUSSION

A. Fitting $H_{c2}(T)$ data

The critical field as a function of temperature, $H_{c2}(T)$, is displayed for a number of alloys in Figs. 2–6 for temperatures $0.5 \text{ K} < T < T_c$. The vertical bars are not error bars per se, but reflect the field transition width (extrapolated 0% to midpoint, see Fig. 1). In general the $H_{c2}(T)$ curves exhibit a negative curvature at low temperatures and high fields, approximating a linear slope as T approaches T_c . In Fig. 2 a qualitative trend in the data is revealed. Graphs of $h^* = H_{c2}(T)/(-dH_{c2}/dt)_{t \text{ near } 1}$ versus $t = T/T_c$ for different alloys are displayed. It can be observed that as the alloy constituents are varied from 3d to 4d to 5d elements the negative curvature at low t decreases. The apparent enhancement of h^* above the Maki limit (equal to 0.693) will be noted. Thus, independent of any fitting procedure, we can conclude that the spin-orbit scattering rate increases with increasing atomic number.

The critical-field data were analyzed via the WHHM theory. A two-parameter fit to the data was performed. The fitting parameters were the Maki paramagnetic limitation parameter α and the spin-orbit scattering parameter $\lambda_{s.o.}$.

The value of α is related to the electronic specific heat γ and the resistivity ρ_n in the normal state:

$$\alpha = 3e^2 \hbar \gamma \rho_n / 2m \pi^2 k_B^2. \quad (1)$$

With additional experimental data (i.e., accurate values for ρ_n and γ) α can thus be determined and the data analysis reduced to a one-parameter fit. Barring such

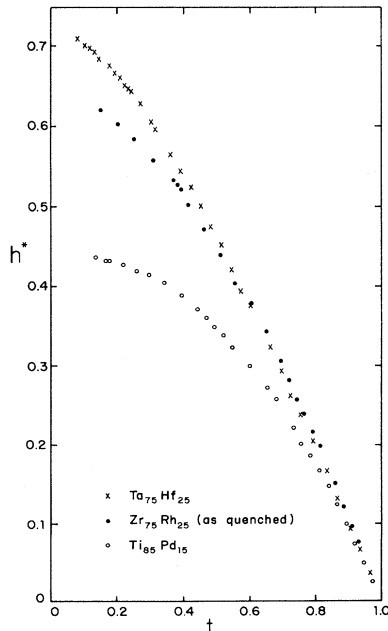


FIG. 2. Reduced-field h^* as a function of reduced temperature t for alloys of the 3d, 4d, and 5d series to illustrate the general trend of h^* at increasing atomic number. Normalization of $H_{c2}(T)$ is carried out using the visual critical-field gradient (see text).

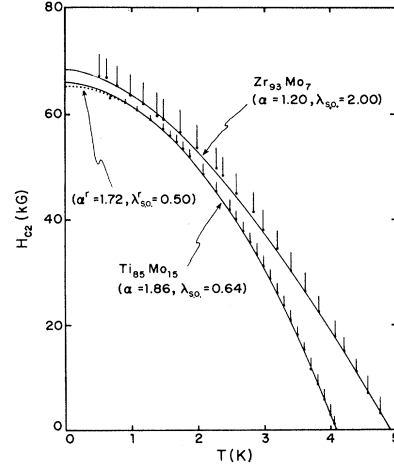


FIG. 3. Upper critical data (0% point) fitted to the WHHM theory for $\text{Ti}_{85}\text{Mo}_{15}$ and $\text{Zr}_{93}\text{Mo}_7$ samples. Vertical bars denote transition widths as defined in Fig. 1. Dotted and solid lines are obtained with and without renormalization correction, respectively. Transition temperatures T_c are the ones obtained at zero field.

data, the analysis remains a two-parameter fit. We have chosen to determine the parameters $\lambda_{s.o.}$ and α utilizing all the data. The $H_{c2}(T)$ data are fitted with the formula provided by WHM,² in terms of digamma functions:

$$\begin{aligned} \ln \frac{1}{t} = & \left[\frac{1}{2} + \frac{i\lambda_{s.o.}}{4\gamma} \right] \psi \left(\frac{1}{2} + (\bar{h} + \frac{1}{2}\lambda_{s.o.} + i\gamma)/2t \right) \\ & + \left[\frac{1}{2} - \frac{i\lambda_{s.o.}}{4\gamma} \right] \psi \left(\frac{1}{2} + (\bar{h} + \frac{1}{2}\lambda_{s.o.} - i\gamma)/2t \right) \\ & - \psi \left[\frac{1}{2} \right], \end{aligned} \quad (2)$$

where $\gamma \equiv [(\alpha\bar{h})^2 - (\frac{1}{2}\lambda_{s.o.})^2]^{1/2}$. Thus

$$\frac{\bar{h}}{(-d\bar{h}/dt)_{t=1}} = \frac{\pi^2 \bar{h}}{4} = \frac{H_{c2}}{(-dH_{c2}/dt)_{t=1}} \quad (3)$$

and

$$\alpha = 5.3 \times 10^{-5} \left[\frac{-dH_{c2}(T)}{dT} \right]_{T=T_c}. \quad (4)$$

Equation (4) offers an approximate value for α if one estimates $[dH_{c2}(T)/dT]_{T_c}$ utilizing data at temperatures near T_c (i.e., finds a visual gradient). We use α deduced from the visual gradient as a guideline in beginning the least-squares fitting routine. The latter is performed on a CDC Cyber 855 computer. A grid search was utilized (to characterize the contours and to avoid local minima) followed by a gradient search method.¹⁰ To find \bar{h} for a given t , α , and $\lambda_{s.o.}$, a bisection method was employed (as t can be a double-valued function of \bar{h} for $\lambda_{s.o.} < \lambda_{s.o.}^c = 0.5319$).² The best fits to the 0% points are represented by the connected lines in Figs. 3–6, and the

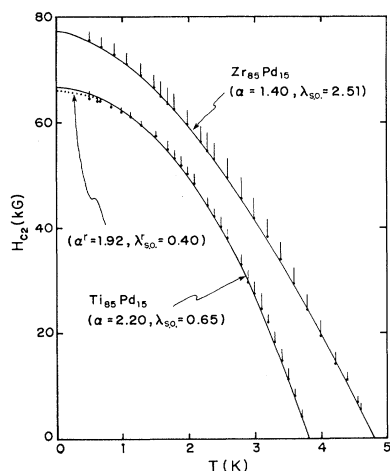


FIG. 4. Same as in Fig. 3 for $\text{Ti}_{85}\text{Pd}_{15}$ and $\text{Zr}_{85}\text{Pd}_{15}$ samples.

values for $\lambda_{s.o.}$ and α are tabulated in Table I. A check on the value of α is provided utilizing data over a limited range ($\sim 0.9 < t \leq 1.0$), by comparing α as deduced from the fitting procedure (α_{fit}) and α as deduced from the visual gradient via Eq. (4) (α_{visual}). The probable error in α as deduced via the slope of $H_{c2}(T)$ near $T = T_c$ depends on the curvature of $H_{c2}(T)$ near T_c , i.e., on the values of $\lambda_{s.o.}$ and α . The curvature of $H_{c2}(T)$ for T near T_c is greater for smaller $\lambda_{s.o.}$ (or larger α values). In fact, we note agreement between α_{fit} and α_{visual} only for very large $\lambda_{s.o.}$, whereas $\alpha_{\text{fit}} \approx 1.19\alpha_{\text{visual}}$ in the case of small $\lambda_{s.o.}$ (or large α) values, as would be expected.

Analysis of our $H_{c2}(T)$ data via the WHHM theory results in good fits, as evidenced by the lines in the figures. We emphasize the fact that we are able to fit *all the data*. The uncertainties in α and $\lambda_{s.o.}$ are limited by the grid size chosen in the fitting procedure. They amount to less than several percent of the values listed in Table I. The $H_{c2}(T)$ data for all the samples (with the exception of a data point in Hf-Mo) we examined fall on or below the theoretical Maki curve (i.e., WHHM curve for $\lambda_{s.o.} = \infty$). Moreover,

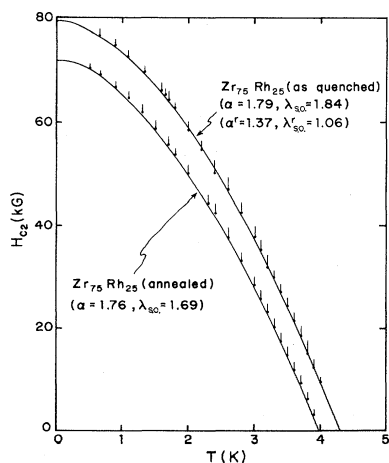


FIG. 5. Same as in Fig. 3 for as-quenched and annealed $\text{Zr}_{75}\text{Rh}_{25}$ samples.

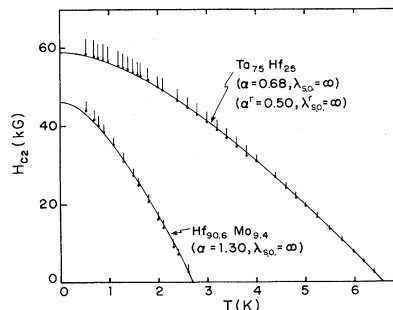


FIG. 6. Same as in Fig. 3 for $\text{Hf}_{90.6}\text{Mo}_{9.4}$ and $\text{Ta}_{75}\text{Hf}_{25}$ samples.

the values of α and $\lambda_{s.o.}$ deduced are of physically reasonable magnitudes. It is important to point out that fitting the midpoints of the transition curves to the WHHM theory also results in good fits. The values of α and $\lambda_{s.o.}$ remain the same.

To emphasize the importance of fitting all the data to the theory in a self-consistent manner and to illustrate the shortcoming of using α_{visual} in the fitting procedure, one is referred to Fig. 7. We illustrate the kind of best fits one can obtain for Ti-Pd and Zr-Rh alloys if one fits the $H_{c2}(T)$ data using α_{visual} . The deficiency of the method is obvious. It results in higher (at least several times) values of $\lambda_{s.o.}$. In cases where $\lambda_{s.o.}$ is large, it can also lead to enhancement of h^* above the Maki limit (equal to 0.693). Another example is given by fitting published $H_{c2}(T)$ data of Ti-V and Ti-Nb (Ref. 11) using the present scheme. Discrepancy between the present $\lambda_{s.o.}$ ($= 0.31$ for Ti-V and 1.28 for Ti-Nb from Table I) values and the published¹¹ $\lambda_{s.o.}$ ($= 0.7$ for Ti-V and 4.5 for Ti-Nb) values is evident. Moreover, excellent fits to the WHHM curves can be obtained. It needs to be pointed out that the procedure of fitting $H_{c2}(T)$ curves with visual critical-field gradient (or α_{visual}) has been customarily used in the literature.

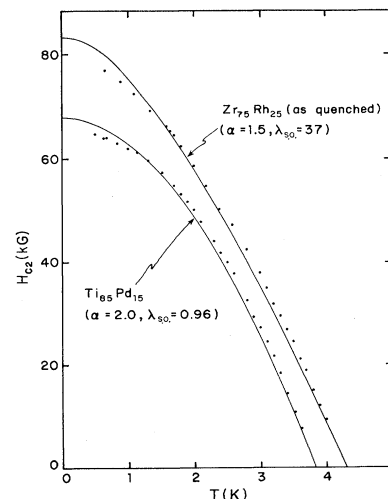


FIG. 7. Same as in Fig. 3 except that visual critical-field gradients are used in $\text{Ti}_{85}\text{Pd}_{15}$ and as-quenched $\text{Zr}_{75}\text{Rh}_{25}$ samples to obtain the best fits (see text).

B. Spin-orbit scattering effects

The WHHM theory assumes that the spin-orbit scattering rate ($1/\tau_{s.o.}$) is much less than the transport scattering rate ($1/\tau_{tr}$). In general we observed [via fits of the $H_{c2}(T)$ data] the ratio $\tau_{s.o.}/\tau_{tr}$ to be much greater than 1. The 3d and 4d alloys examined revealed values of $\lambda_{s.o.} < 3$, i.e., $\tau_{s.o.} > 10^{-13}$ sec, [$\tau_{s.o.} = 2\hbar(3\pi k_B T_c \lambda_{s.o.})^{-1}$].² An estimation of τ_{tr} can be achieved via⁴ $\tau_{tr} \approx 2 \times 10^8 \gamma_v [\rho_n n^{4/3} (S/S_f)^2]^{-1}$, where n is the effective conduction-electron density and S/S_f the ratio of free Fermi-surface area S to that of a free-electron gas of density n . Assuming $S/S_f \sim 0.6$ in alloys with $\rho_n \gtrsim 100 \mu\Omega \text{ cm}$, one finds in general $\tau_{tr} \lesssim 10^{-15}$ sec.¹² Thus the assumption $\tau_{s.o.}/\tau_{tr} \gg 1$ is well satisfied. In the case of the 5d alloys examined $\lambda_{s.o.} > 10$, and the fits are not very sensitive to a large variation of $\lambda_{s.o.}$, i.e., $10 < \lambda_{s.o.} < \infty$. Therefore, one cannot definitely evaluate $\tau_{s.o.}/\tau_{tr}$. But we can evaluate the $H_{c2}(T)$ data via the WHHM theory with the confidence that the $H_{c2}(T)$ curve is bounded closely above (see Fig. 6) by the Maki curve ($\lambda_{s.o.} = \infty$). That is, it is sufficient basis to the conclusions we present herein to know that $10 < \lambda_{s.o.} < \infty$ for the 5d alloys.

We note a correlation between increasing values of $\lambda_{s.o.}$ and increasing atomic number Z for the transition-metal alloys examined (see Table I). Further insight may be gained via the relation²

$$\frac{3\pi k_B T_c \lambda_{s.o.}}{2\hbar} = \frac{1}{\tau_{s.o.}} = \frac{8\pi}{3\hbar} n_i N_b(0) |\langle \mathcal{M} \rangle_{s.o.}|^2, \quad (5)$$

where n_i is the density of spin-orbit scattering centers and $N_b(0)$ is the bare density of states and $\langle \mathcal{M} \rangle_{s.o.}$ is the matrix element associated with spin-orbit scattering. We cannot precisely determine n_i or $N_b(0)$ for all the alloys examined, but we do expect the variation in $|\langle \mathcal{M} \rangle_{s.o.}|^2$ with Z to dominate changes in $\lambda_{s.o.} T_c$. [See Table II for some values of $N_b(0)$.] We compare $\lambda_{s.o.} T_c$ with values of spin-orbit coupling parameter ξ_d for the d band determined in single-crystal calculations.¹³ As can be seen in Table I, $\lambda_{s.o.} T_c$ and ξ_d^2 scale roughly at the same rate, as we move down the Periodic Table, from 3d to 5d binary alloys.

TABLE II. Superconducting parameters for five alloys selected to study the effect of renormalization. The density (except Zr-Rh) is taken as the average density of the components in the alloys. sf denotes spin fluctuation.

Alloys	Θ_D (K)	M (g)	d (g/cm ³)	λ_{e-ph}	λ_{sf}	$N_b(0)$ (states/eV atom spin)	\bar{I}	α/α'	α'	$\lambda_{s.o.}^r$
Ti ₄₂ V ₅₈	270 ^a	50.0	5.4	1.4	0.41	0.89	0.61	1.14	1.62	0.14
Ti ₈₅ Mo ₁₅	295 ^b	55.1	5.4	0.87	0.21	0.71	0.49	1.07	1.72	0.50
Ti ₈₅ Pd ₁₅	295 ^c	56.7	5.6	0.67	0.09	0.53	0.36	1.15	1.92	0.40
Zr ₇₅ Rh ₂₅	191 ^d	94.1	7.6 ^e	0.88	0.16	0.60	0.37	1.31	1.37	1.06
Ta ₇₅ Hf ₂₅	200 ^f	180	15.7	0.99	0.15	0.54	0.37	1.36	0.50	∞

^aC. H. Cheng, K. P. Gupta, E. V. van Reuth, and Paul A. Beck, Phys. Rev. 126, 2030 (1962).

^bE. W. Collings, J. C. Ho, and R. I. Jaffe, Phys. Rev. B 5, 4435 (1972).

^cWe assume it has similar value as in the Ti-Mo alloy.

^dP. Garoche and W. L. Johnson, Solid State Commun. 39, 403 (1981).

^eA. J. Drehman and W. L. Johnson, Phys. Status Solidi A 52, 499 (1974).

^fE. Bucher, F. Heiniger, J. L. Olsen, and J. Müller, in *Proceedings of the 9th International Conference on Low Temperature Physics* (Plenum, New York, 1964), p. 616.

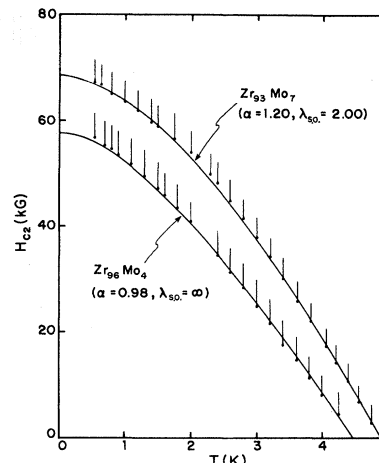


FIG. 8. Same as in Fig. 3 for Zr₉₆Mo₄ and Zr₉₃Mo₇ samples to illustrate the effect of sample inhomogeneity on the values of $\lambda_{s.o.}$.

An estimate of $\tau_{s.o.}$ can be made from Eq. (5) using the values of ξ_d in Ref. 13. For Ti and Zr, $\xi_d \approx 0.02$ and 0.06 eV, respectively. The $N_b(0)$ values for Ti- and Zr-based alloys are taken from Table I. Assuming all the Ti and Zr sites are scattering centers, we find $\tau_{s.o.} \approx 3.6 \times 10^{-13}$ and 4×10^{-14} sec for Ti and Zr alloys, respectively. On the other hand, using our tabulated values of $\lambda_{s.o.}$ and T_c , we obtain $\tau_{s.o.} \approx 5.8 \times 10^{-13}$ sec for Ti₈₅Pd₁₅ and 2.1×10^{-13} sec for Zr₇₅Rh₂₅ alloys. Considering that n_i is not well defined for concentrated alloys, the agreement is qualitatively satisfactory.

It should be noted that the $\lambda_{s.o.}$ values obtained for the 3d and 4d alloys via the present scheme range from 0.28 to 2.51 (see Table I). This can be compared with the values for Ti- and Zr-based superconductors given in Table II of Ref. 12 ($2 < \lambda_{s.o.} < 6$). Thus relatively low values of $\lambda_{s.o.}$ are obtained without taking into account renormalization effects if *all the data* are fitted to the WHHM theory. An attempt is also made to determine the effect of sample inhomogeneity on the values of $\lambda_{s.o.}$ via a study of two metastable Zr-Mo alloys (see Fig. 8).

The first alloy considered, $Zr_{93}Mo_7$, is stable in the β phase,⁷ whereas $Zr_{96}Mo_4$ is on the phase boundary between α -, β -, and ω -Zr. X-ray diffraction reveals the presence of α - and ω -Zr in the $Zr_{96}Mo_4$ alloy only. Furthermore, it can be noted that the superconducting transition from 0% point to midpoint on the resistivity curve of $Zr_{93}Mo_7$ is narrower (~ 200 mK) and sharper than that of $Zr_{96}Mo_4$ (~ 400 mK).

When $H_{c2}(T)$ is examined for $Zr_{93}Mo_7$ values of $\alpha=2.0$ and $\lambda_{s.o.}=1.9$ are found via the WHHM analysis. The value of $\lambda_{s.o.}T_c=9.8$ is of the same order of magnitude as the other $4d$ alloys considered. However, $H_{c2}(T)$ for the $Zr_{96}Mo_4$ alloy displays large value for $\lambda_{s.o.}$ ($\lambda_{s.o.}=\infty$). We interpret this result as possible further evidence of the influence of inhomogeneity of a sample upon its critical-field behavior.¹⁴ On the other hand, results on $Zr_{75}Rh_{25}$ annealed at 550 K for 68 h are very similar to the as-quenched sample (see Table I). The transition width remains very sharp (~ 5 mK).

C. Renormalization and strong coupling corrections

Recently, evidence has been presented to the effect that electron-phonon and electron-electron interactions will decrease the Pauli limiting field, and lack of consideration of these effects will result in enormously large values of spin-orbit scattering rates.^{4,6} It was concluded that only by inclusion of these effects could $H_{c2}(T)$ data for Nb_3Sn reasonably be fitted and it was stated that even in weak coupled superconductors the effects of electron-phonon renormalizations of normal-state parameters could be significant. Although we are able to fit our data quite reasonably within the auspices of the unrenormalized WHHM theory, we attempt to take this one step further by performing the renormalization procedure as suggested by Orlando and Beasley⁴ for our $H_{c2}(T)$ data for a number of samples. We thus obtained values for the spin-orbit interaction parameter, renormalized ($\lambda_{s.o.}^r$) and the paramagnetic limitation parameter, renormalized (α^r), as well as values for λ_{e-ph} and λ_{sf} (the mass renormalizations from the electron-phonon and electron-electron interactions). Comparison can then be made with the "bare" values.

The renormalization procedure is based upon the enhancement of the Pauli limiting field H_p^{BCS} by electron-phonon and electron-electron [and the related Stoner enhancement factor $1/(1-\bar{I})$] many-body corrections. The enhancement is quantified:

$$H_p = (1 + \lambda_{e-ph} + \lambda_{sf})(1 - \bar{I})H_p^{BCS}. \quad (6)$$

With values for λ_{e-ph} , λ_{sf} , and \bar{I} we substitute α^r for α in Eq. (2), where we obtain α^r

$$\alpha^r = \frac{\alpha}{(1 + \lambda_{e-ph} + \lambda_{sf})(1 - \bar{I})}, \quad (7)$$

and redo the fits to the $H_{c2}(T)$ curves, where α is given in Eq. (4). The values of λ_{e-ph} , λ_{sf} , and \bar{I} are deduced from the T_c , magnetic susceptibility, and mass enhancement equations:

$$T_c = \frac{\Theta_D}{1.45} \exp \left[- \frac{1 + \lambda_{e-ph} + \lambda_{sf}}{\lambda_{e-ph} - \lambda_{sf} - \mu^*} \right], \quad (8)$$

$$\lambda_{sf} = \frac{9}{2} \bar{I} \ln \left[1 + \frac{P_1^2}{12} \frac{\bar{I}}{1 - \bar{I}} \right], \quad (9)$$

$$\begin{aligned} N^{\gamma}(0) &= (1 + \lambda_{e-ph} + \lambda_{sf})N_b(0) \\ &= 9.46 \times 10^{-10} \frac{M}{\rho_n d} \left[- \frac{dH_{c2}}{dT} \right]_{T=T_c}, \end{aligned} \quad (10)$$

$$\chi_v = \frac{\mu_B^2 N_b(0)}{1 - \bar{I}}, \quad (11)$$

where d is the density, Θ_D is the Debye temperature, P_1 is a momentum cutoff parameter, and μ^* is taken to be 0.13. We do not deduce \bar{I} from experimental measurements of magnetic susceptibility as we are not able to separate the valence and Van Vleck terms; we instead depend upon values for the elements, calculated by Janak.¹⁵ Janak actually supplies values of I , related to \bar{I} via

$$\bar{I} = 2N_b(0)I. \quad (12)$$

It is found that the value of I ($\simeq 0.3$ eV) is almost constant for the refractory metals.¹⁵ Moreover, the theoretical Stoner enhancement factor also compares favorably with its experimental counterpart.¹⁶ For the alloys, we have checked the experimental value of the Stoner enhancement factor in amorphous $Zr_{72}Cu_{28}$ corrected for the Van Vleck term.¹⁷ It agrees with the theoretical value (~ 1.6) obtained using $N_b(0) \simeq 0.55$ states/eV atom spin from specific-heat data¹⁸ and $I = 0.34$ eV from Janak.¹⁵ The values for momentum cutoff P_1 (expressed as a fraction of the Fermi momentum) for Nb and V are obtained from the theoretical results of Ref. 16 and Eq. (9). Assuming that the neighboring refractory metals (e.g., Ti, Zr, Hf, Ta) have similar P_1 values for each series, we take $(P_1^2)_{3d} \simeq 1.2$, $(P_1^2)_{4d} \simeq (P_1^2)_{5d} \simeq 2$. Values of Θ_D in general are obtained from the literature (see Table II).

Knowing the *actual* critical-field gradient, Θ_D , T_c , one can solve for \bar{I} , λ_{e-ph} , λ_{sf} , $N_b(0)$ using Eqs. (8)–(10) and (12). Therefore, we can employ the grid-searching scheme discussed above to carry out the two-parameter fit to include renormalization effects. This is done for only five alloys where specific-heat data are available. We find that the quality of the fit to the data is also excellent. Results for some of the alloys are illustrated by dotted lines in the figures. The relevant parameters are listed in Table II. Values of renormalized spin-orbit scattering parameters are somewhat (at most by a factor of 2) reduced from the bare values. The trend of $\lambda_{s.o.}$ remains unchanged.

Until now, a theory which incorporates both renormalization and strong-coupling corrections has not been developed. In the case of very strong spin-orbit scattering ($\lambda_{s.o.} \rightarrow \infty$), Rainer and Bergmann³ calculated the enhancement of $H_{c2}(T)$ for several typical electron-phonon spectra. They quantified the enhancement by a parameter $\eta_{H_{c2}}(T) = H_{c2}(T)/H_{c2}^{BCS}(T)$. Results at $T=0$ and T_c were given for the Debye model as a function of $T_c/\langle\omega\rangle$, where $\langle\omega\rangle$ is the average phonon frequency. The function $\eta_{H_{c2}}(T) \simeq 1$ was found to increase as a func-

tion of temperature. Assuming that this trend holds for our samples, the $H_{c2}^{\text{BCS}}(T)$ data to be fitted to the WHHM theory will tend to follow a curve with decreasing curvature towards T_c . The latter tends to increase the value of $\lambda_{s.o.}^r$ in the curve-fitting procedure. On the other hand, a reduced field gradient at T_c also decreases the value of α^r and thus the value of $\lambda_{s.o.}^r$. To examine the overall effect more quantitatively, we divide our $H_{c2}(T)$ data by an extrapolated function $\eta_{H_{c2}}(t) \simeq 1.06 + 0.05t$, a form compatible with typical $T_c/\langle\omega\rangle$ values.³ Curve fitting to the corrected $H_{c2}(T)$ data results in $\lambda_{s.o.}^r = 0.12$ for Ti-V, 1.3 for Zr-Rh, and ∞ for Ta-Hf alloys. Therefore, the net effect due to strong coupling correction on the values of $\lambda_{s.o.}^r$ (see Table II) might be small.

IV. SUMMARY AND CONCLUSION

We have measured in detail ($H \leq 90$ kG, $T_c > T > 0.5$ K) the upper critical fields in several liquid-quenched metastable superconductors. Analysis is performed within the framework of the WHHM theory using all the data (weighted equally) in a two-parameter ($\alpha, \lambda_{s.o.}$) curve-fitting procedure. Excellent fits are obtained. The spin-orbit scattering parameter $\lambda_{s.o.}$ is found to be smaller

than ~ 2.5 for the $3d$ and $4d$ alloys. Sample inhomogeneity is found to increase the $\lambda_{s.o.}$ value significantly. Otherwise, no enhancement (with the exception of one data point in Hf-Mo) of $H_{c2}(T)$ above the Maki curve ($\lambda_{s.o.} = \infty$) is observed. The spin-orbit scattering time is compared favorably to data obtained from band-structure calculation. An attempt is made to include both renormalization and strong coupling corrections in the data analysis. The overall effect reduces the value of $\lambda_{s.o.}$ by at most a factor of ~ 2 in our samples. The relative insensitivity of renormalization correction in our alloys is probably due to the mutually compensating factors $(1 + \lambda_{e-ph} + \lambda_{sf})$ and $(1 - \bar{I})$. Also, in bulk samples, orbital pair breaking already plays a major role in determining the upper critical field. This is different in thin films¹⁹ where renormalization correction can have a very important effect on the value of $\lambda_{s.o.}$.

ACKNOWLEDGMENTS

The authors thank Dr. T. P. Orlando for useful discussions. They also are indebted to Dr. B. Deaver for providing them with the crucial electronic parts of the temperature controller. This research is sponsored by the National Science Foundation Grant No. DMR-83-02624.

*Present address: Ames Laboratory, U.S. DOE, Ames, IA 50011.

† Present address: W. M. Keck Laboratory, California Institute of Technology, Pasadena, CA 91125.

¹K. Maki, *Physica* (N.Y.) **1**, 127 (1964); K. Maki, *Phys. Rev.* **148**, 362 (1966).

²N. R. Werthamer, E. Helfand, and P. C. Hohenberg, *Phys. Rev.* **147**, 295 (1966); E. Helfand and N. R. Werthamer, *ibid.* **147**, 288 (1966).

³D. Rainer and G. Bergmann, *J. Low Temp. Phys.* **14**, 501 (1974).

⁴T. P. Orlando, E. J. McNiff, Jr., S. Foner, and M. R. Beasley, *Phys. Rev. B* **19**, 4545 (1979); T. P. Orlando and M. R. Beasley, *Phys. Rev. Lett.* **46**, 1598 (1981).

⁵W. Hänsch, *Phys. Rev. B* **29**, 446 (1984).

⁶T. P. Orlando, in *Superconductivity in d- and f-Band Metals*, edited by W. Buckel and W. Weber (Kernforschungszentrum, Karlsruhe GmbH, 1982) p. 75, and references therein.

⁷S. J. Poon and T. E. Dowling, *Solid State Commun.* **50**, 189 (1984); S. J. Poon, *ibid.* **47**, 431 (1983).

⁸The Ge semiconductor thermometer and calibration were ob-

tained from Lakeshore Cryotronics, Inc., Westerville, Ohio.

⁹A. C. Rose-Innes, *Low-Temperature Techniques* (The English Universities Press Limited, London, 1964).

¹⁰P. R. Bevington, *Data Reduction and Error Analysis for the Physical Sciences* (McGraw-Hill, New York, 1969), p. 204.

¹¹L. J. Neuringer and Y. Shapira, *Phys. Rev. Lett.* **17**, 81 (1966).

¹²M. G. Karkut and R. R. Hake, *Phys. Rev. B* **28**, 1396 (1983).

¹³O. Jepsen, O. Krogh Andersen, and A. R. Mackintosh, *Phys. Rev. B* **12**, 3084 (1975).

¹⁴S. J. Poon, S. K. Hasanain, and K. M. Wong, *Phys. Rev. Lett.* **A 93**, 495 (1983), and references therein.

¹⁵J. F. Janak, *Phys. Rev. B* **16**, 255 (1977).

¹⁶H. Rietschel and H. Winter, *Phys. Rev. Lett.* **43**, 1256 (1979); H. Rietschel, H. Winter, and W. Reichardt, *Phys. Rev. B* **22**, 4284 (1980).

¹⁷H. J. Eifert, B. Elschner, and K. H. J. Buschow, *Phys. Rev. B* **25**, 7441 (1982).

¹⁸K. Samwer and H. v. Löhneysen, *Phys. Rev. B* **26**, 107 (1982).

¹⁹P. M. Tedrow, J. T. Kucera, D. Rainer, and T. P. Orlando, *Phys. Rev. Lett.* **52**, 1637 (1984); also private communication.